New versatile ligand family, pyrazine-modulated oligo-α-pyridylamino ligands, from coordination polymer to extended metal atom chains†

Rayyat Huseyn Ismayilov,[a,b] Wen-Zhen Wang,[a,b] Gene-Hsiang Lee,[a] Rui-Ren Wang,[a] Isiah Po-Chun Liu,[a,b] Chen-Yu Yeh[c] and Shie-Ming Peng*[a,b]

Received 12th January 2007, Accepted 13th April 2007
First published as an Advance Article on the web 9th May 2007
DOI: 10.1039/b700533d

Here we designed and synthesized a new ligand, di(2-pyrazyl)amine (Hdpza) (**1**) and studied its coordination modes and the corresponding complexes with Cu(II), Co(II), Ni(II) and Cr(II). Hdpza is an analogue of the well-studied di(2-pyridyl)amine (Hdpa) ligand, which was used to generate the first extended metal atom chain. Three types of coordination modes were found: *anti–anti* style which resulted in a mononuclear compound $[Cu(Hdpza)_2(H_2O)_2](ClO_4)_2$ (**2**); *anti–syn* which was observed in a complex for the first time and resulted in a 2-D coordination polymer $[Co(\mu_2\text{-}Hdpza)_2(NCS)_2]$ (**3**); and *syn–syn* type which was observed in extended metal atom chains $[Ni_3(\mu_3\text{-}dpza)_4Cl_2]$ (**4**), $[Ni_3(\mu_3\text{-}dpza)_4(NCS)_2]$ (**5**) and $[Cr_3(\mu_3\text{-}dpza)_4Cl_2]$ (**6**). Weak antiferromagnetic coupling *via* Hdpza was observed in **3**, whereas magnetic studies on extended metal atom chains **4** and **5** revealed that the interaction parameter was more than $-200\ cm^{-1}$. Electrochemistry showed that the extended metal atom chains **4–6** are much more stable to oxidation than the Hdpa complexes, and are able to undergo reduction.

Introduction

In the past decade, by employing oligo-α-pyridylamino ligands (Scheme 1), a series of tri-,[1,2] tetra-,[3] penta-,[4] hexa-,[5] hepta-,[3a,6] and nona-[7]nuclear extended metal atom chains (EMACs) have been synthesized. The structures and properties that have been found are invaluable for acquiring a fundamental understanding of metal–metal bonds and promising for potential applications such as molecular metal wires and switches.[8] In nickel EMACs, both terminal nickel atoms are five-coordinated high spin nickel(II), whereas the inner nickel atoms are four-coordinated and diamagnetic. The complexes are actually an anti-ferromagnetically coupling dinuclear species. Three to nine nickel EMAC have been obtained so far, and their coupling constants (J) have been found to decrease with an increase in distance between the two terminal nickel atoms.[7a,9] In cobalt(II) and chromium(II) trimetal EMACs, two kinds of structures have been found: symmetrical (delocalized) and unsymmetrical (localized) configurations. In the former structure, metal–metal distances are the same or very close and every metal atom is bonded with a neighboring metal(s). In the latter structure, two different metal–metal distances have been observed: a strong metal–metal bond between a pair of metal atoms linked closely with a third metal atom separated by some distance from the other two.[2a,2c] Furthermore, a structural change between localized and delocalized electron configuration was observed when the extended metal atom chains were oxidized, which is crucial to enable the complexes to function as molecular switches and wires.[2e] Compounds with different redox properties are especially interesting in molecular device applications. However research in this field has been restricted by difficulties with syntheses. EMACs for some first row transition metals, for instance, iron and manganese have yet to be successfully synthesized. The longest EMAC molecules so far obtained have contained nine metal atoms for nickel[7a] and chromium,[7b] and seven for cobalt complexes.[6c] Great efforts have been made in our group to expand the variety of metals and lengths of EMACs. Recently we designed a series of pyrazine-modulated oligo-α-pyridylamino ligands, by including pyrazine instead of pyridine ring(s) in oligo-α-pyridylamino ligands.[10] The introduction of one or more of the nitrogen-rich aromatic rings such as pyrazine to the ligands, significantly improved the reactivity leading to the EMAC, and resulted in complexes with very different redox properties (Scheme 1). Furthermore, by providing more donor nitrogen atoms in aromatic ring(s), the pyrazine ligands exhibit more coordination forms and are especially versatile in the construction of coordination polymers.[10,11] Here we report for the first time the syntheses of the novel pyrazine-modulated ligand, di(2-pyrazyl)amine (Hdpza) (**1**), its copper complex $[Cu(Hdpza)_2(H_2O)_2](ClO_4)_2$ (**2**), its 2-D cobalt complex $[Co(\mu_2\text{-}Hdpza)_2(NCS)_2]$ (**3**), and its EMACs $[Ni_3(\mu_3\text{-}dpza)_4Cl_2]$ (**4**), $[Ni_3(\mu_3\text{-}dpza)_4(NCS)_2]$ (**5**) and $[Cr_3(\mu_3\text{-}dpza)_4Cl_2]$ (**6**).

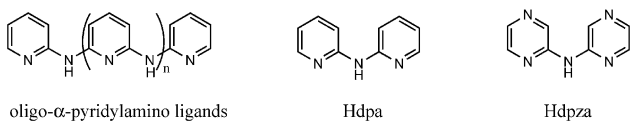

Scheme 1

[a]*Department of Chemistry, National Taiwan University, Taipei, Taiwan. E-mail: smpeng@ntu.edu.tw*
[b]*Institute of Chemistry, Academia Sinica, Taipei, Taiwan*
[c]*Department of Chemistry, National Chung Hsing University, Taichung, Taiwan*

† The HTML version of this article has been enhanced with colour images.

Results and discussion

Syntheses and structures

The ligand Hdpza **1** was synthesized on the basis of Buchwald's palladium-catalyzed procedures *via* the coupling of aminopyrazine and chloropyrazine,[12] characterized by X-ray crystallography, IR, ^{1}H NMR and MS(FAB). The crystal structure of Hdpza is shown in Fig. 1. Selected bond lengths and angles are listed in Table 1. Three possible configurations resulting from different orientations of pyrazine rings were expected, and the crystal structure of Hdpza showed that the free ligand adopts the *anti–syn* configuration (Scheme 2). Hydrogen bonds are formed between N2 and N4 (2.944 Å), which link the ligand to a 1-D network along the *a* axis (Fig. 1(b)). The 1-D chains stack parallel with each other along the *b* axis at a distance of 3.731 Å, indicating a strong π–π interaction between pyrazine rings.

Table 1 Selected bond lengths (Å) and angles (°) for **1–3**

Di(pyrazin-2-yl)amine (Hdpza) (**1**)			
N(1)–C(1)	1.342(4)	N(1)–C(4)	1.339(3)
N(2)–C(4)	1.380(3)	N(2)–C(5)	1.376(3)
N(3)–C(5)	1.320(3)	N(3)–C(8)	1.346(3)
N(4)–C(2)	1.335(4)	N(4)–C(3)	1.324(3)
N(5)–C(6)	1.309(3)	N(5)–C(7)	1.340(4)
C(1)–C(2)	1.359(4)	C(3)–C(4)	1.394(3)
C(5)–C(6)	1.414(3)	N(7)–C(8)	1.360(4)
C(1)–N(1)–C(4)	115.7(2)	C(4)–N(2)–C(5)	128.63(19)
C(5)–N(3)–C(8)	116.3(2)	C(2)–N(4)–C(3)	117.0(2)
C(6)–N(5)–C(7)	117.0(2)		
$[Cu(Hdpza)_2(H_2O)_2](ClO_4)_2$ (**2**)			
Cu–N(1)	2.016(2)	Cu–N(4)	2.043(2)
Cu–O(1)	2.354(2)		
N(1)–Cu–N(1A)	180.00(4)	N(1)–Cu–N(4)	94.21(8)
N(1)–Cu–N(4A)	85.79(8)	N(1)–Cu–O(1)	90.40(9)
N(1)–Cu–O(1A)	89.60(9)	N(1A)–Cu–N(4)	85.79(8)
N(4)–Cu–N(4A)	180.00(12)	N(4)–Cu–O(1)	90.49(8)
N(4)–Cu–O(1A)	89.51(8)	O(1)–Cu–O(1A)	180.00(10)
$[Co(\mu_2\text{-}Hdpza)_2(NCS)_2]$ (**3**)			
Co–N(1)	2.220(5)	Co–N(5B)	2.184(5)
Co–N(5B)	2.184(5)	Co–N(6)	2.073(5)
N(1)–Co–N(1A)	180.0(4)	N(1)–Co–N(5B)	87.20(19)
N(1)–Co–N(5C)	92.80(19)	N(1)–Co–N(6)	91.6(2)
N(1)–Co–N(6A)	88.4(2)	N(1A)–Co–N(5B)	92.80(19)
N(1A)–Co–N(5C)	87.20(19)	N(1A)–Co–N(6)	88.4(2)
N(1A)–Co–N(6A)	91.6(2)	N(5B)–Co–N(5C)	180.00(10)
N(5B)–Co–N(6)	89.0(2)	N(5C)–Co–N(6)	91.0(2)
N(5B)–Co–N(6A)	91.0(2)	N(5C)–Co–N(6A)	89.0(2)
N(6)–Co–N(6A)	180.0(3)		

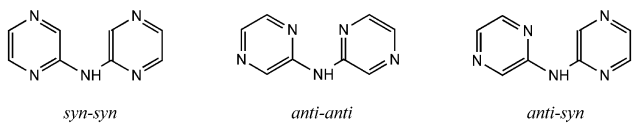

Scheme 2

The complexes $[Cu(Hdpza)_2(H_2O)_2](ClO_4)_2$ (**2**) and $[Co(\mu_2\text{-}Hdpza)_2(NCS)_2]$ (**3**) were synthesized by direct reactions of Hdpza with $Cu(ClO_4)_2{\cdot}6H_2O$ and $Co(NCS)_2$ in methanol, respectively. The crystal structures are shown in Fig. 2 and 3 and selected bond lengths and angles are listed in Table 1. In complex **2** Hdpza coordinates to Cu(II) as a bidentate ligand with 1-, and 1′-nitrogen atoms of pyrazine in *anti–anti* conformation (Scheme 2),[1a] and the amino nitrogen atom is free. Cu(II) is six-coordinated to four nitrogen atoms from pyrazine and two oxygen atoms from water molecules. The coordination geometry is an elongated

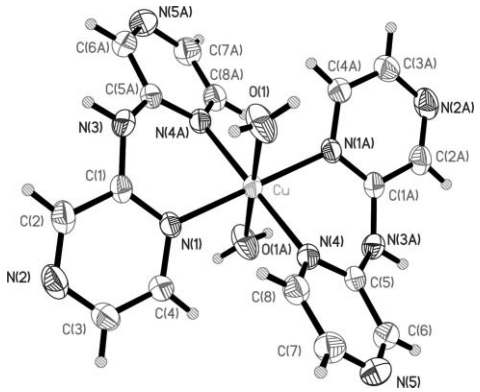

Fig. 2 Crystal structure of $[Cu(Hdpza)_2(H_2O)_2](ClO_4)_2$ in $2{\cdot}2H_2O$. Thermal ellipsoids are at the 50% probability level. The hydrogen atoms have been omitted for clarity. Symmetry operations A = $-x$, $-y-1$, $-z$.

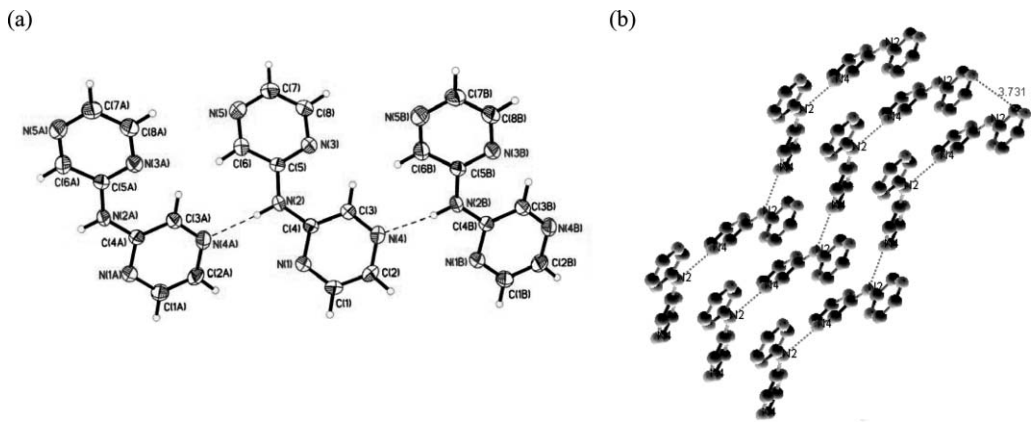

Fig. 1 (a) Crystal structure of Hdpza (**1**). Thermal ellipsoids are at the 50% probability level. The hydrogen atoms have been omitted for clarity. (b) Stacking of 1-D chains of Hdpza *via* hydrogen bonds. Symmetry operations A = $x-1/2$, $-y$, z and B = $x+1/2$, $-y$, z.

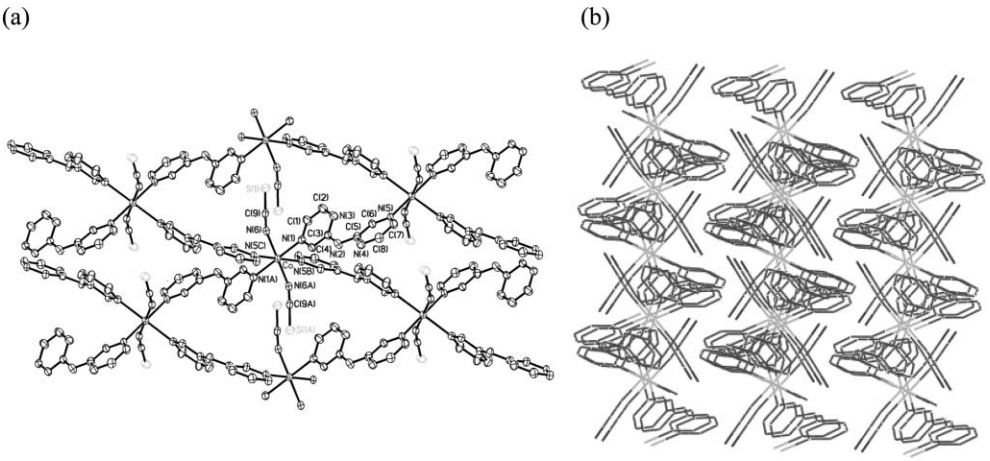

Fig. 3 (a) Crystal structure of $[Co(\mu_2\text{-Hdpza})_2(NCS)_2]$ (**3**). The hydrogen atoms have been omitted for clarity and thermal ellipsoids are at the 50% probability level. (b) Stacking of the wavy planes in **3**. Symmetry operations A = $-x$, $-y$, $-z$; B = $-x - 1/2$, $y + 1/2$, $-z + 1/2$ and C = $x + 1/2$, $-y - 1/2$, $z - 1/2$.

Table 2 Hydrogen bond distances (Å) for complex $[Cu(Hdpza)_2(H_2O)_2](ClO_4)_2$ in **2**·$2H_2O$

O(1)···H···N(2)	2.892	O(1)···H···O(21)	2.754
O(21)···H···O(14)	2.914	N(3)···H···O(11)	2.910

octahedron with Cu(II) atom lying on an inversion centre and water molecules at the axial positions. Extensive hydrogen bonds between nitrogen atoms, perchlorate anions and water molecules are observed, giving rise to the 3-D network of the compound (Table 2).

Complex $[Co(\mu_2\text{-Hdpza})_2(NCS)_2]$ **3** is a two dimensional coordination polymer, consisting of [2 × 2] square-grids. The layers of 2-D structure in **3** are severely distorted and actually form wavy planes. The coordination geometry is octahedron with Co(II) sitting on the inversion center. The Co(II) is six-coordinated to four nitrogen atoms of pyrazine from four different ligands and two nitrogen atoms from a NCS^- anion. The Hdpza ligand coordinates to the Co(II) as a bidentate bridging ligand with every pyrazine ring providing one 4-, or 4′-nitrogen atom. The amino nitrogen atom is free. It is noticeable that Hdpza adopts an *anti–syn* conformation (Scheme 2), which was reported for the hydrogen bonds of free ligand Hdpa.[1a] Compound **3** provides the first example of an *anti–syn* style complex. There are no solvent molecules present in the crystal lattice, nor hydrogen bonds or π–π interactions.

The chloride complexes $[M_3(\mu_3\text{-dpza})_4Cl_2]$ (M=Ni (**4**), Cr(**6**)) were synthesized by the reaction of anhydrous MCl_2 with Hdpza ligand in an argon atmosphere employing naphthalene as the solvent and Bu^tOK as base to deprotonate the amine group. Our thiocyanate species $[Ni_3(\mu_3\text{-dpza})_4(NCS)_2]$ (**5**) was obtained through the substitution of axial chloride ligands from **4**. The crystal structures of **4–6** are shown in Fig. 4–6, and are essentially similar to oligo-α-pyridylamino EMACs.[2c,2f] The molecules are linear with M–M–M bond angles in the range of 177–180° and chloride or nitrogen atoms of axial ligands bonded to the terminal metal collinear with the M_3 axis (Table 3). Amino nitrogen, 1- and 1′-nitrogen atoms of pyrazine are coordinated to the metal, thus the ligand is coordinated as a tridentate anion in a *syn–syn* form (Scheme 2). There are two independent molecules in both

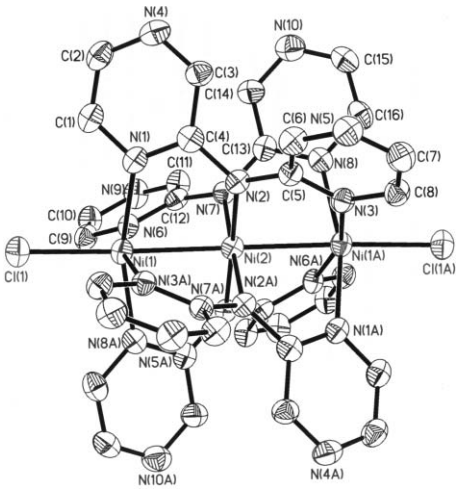

Fig. 4 Crystal structure of one $[Ni_3(\mu_3\text{-dpza})_4Cl_2]$ molecule in **4**·$0.75C_4H_{10}O$·$0.25CH_2Cl_2$. The hydrogen atoms have been omitted for clarity and thermal ellipsoids are at the 50% probability level. Symmetry operations A = $-x + 1$, y, $-z + 1/2$.

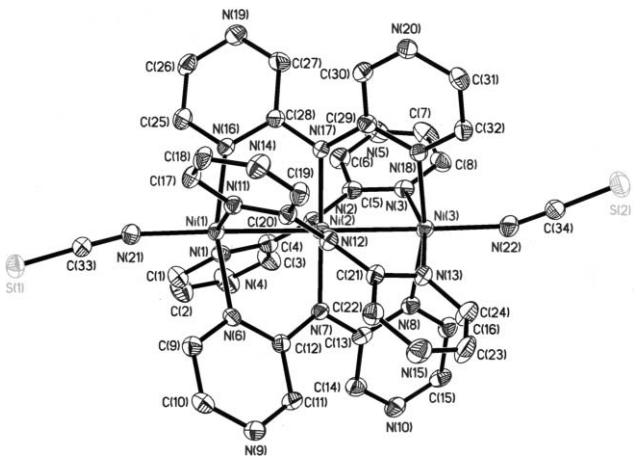

Fig. 5 Crystal structure of $[Ni_3(\mu_3\text{-dpza})_4(NCS)_2]$ in **5**·$0.5H_2O$. The hydrogen atoms have been omitted for clarity and thermal ellipsoids are at the 50% probability level.

Table 3 Selected bond distances (Å), angles (°) and torsion angles (°) for complexes **4–6**

$[Ni_3(\mu_3\text{-dpza})_4Cl_2]$(**4**)[a]			
Ni(1)–Ni(2)	2.4464(5)	Ni(1)–Cl(1)	2.2934(12)
Ni(3)–Ni(4)	2.4393(5)	Ni(3)–Cl(2)	2.3035(10)
Ni(1)–N_{av}[b]	2.091(3)	Ni(2)–N_{av}[b]	1.885(3)
Ni(3)–N_{av}[b]	2.091(3)	Ni(4)–N_{av}[b]	1.888(3)
Ni(1)–Ni(2)–Ni(1A)	178.08(4)	Ni(3)–Ni(4)–Ni(3B)	179.02(4)
C1(1)–Ni(1)–Ni(2)	178.05(4)	Cl(2)–Ni(3)–Ni(4)	179.62(4)
N–Ni–Ni–N Torsion$_{av}$[b]	24.51		
$[Ni_3(\mu_3\text{-dpza})_4(NCS)_2]$ (**5**)			
Ni(1)–Ni(2)	2.4400(8)	Ni(2)–Ni(3)	2.4417(8)
Ni(1)–N(21)	1.980(4)	Ni(3)–N(22)	1.979(5)
Ni(1)–N_{av}[b]	2.079(4)	Ni(2)–N_{av}[b]	1.892(4)
Ni(3)–N_{av}[b]	2.074(4)		
Ni(1)–Ni(2)–Ni(3)	179.10(3)	N(21)–Ni(1)–Ni(2)	178.68(12)
Ni(2)–Ni(3)–N(22)	177.92(13)		
N–Ni–Ni–N Torsion$_{av}$[b]	23.14		
$[Cr_3(\mu_3\text{-dpza})_4Cl_2]$(**6**)[c]			
Cr(1)–Cr(2)	2.3846(9)	Cr(1)–Cl(1)	2.4462(16)
Cr(3)–Cr(4)	2.3957(8)	Cr(3)–C1(2)	2.4860(16)
Cr(1)–N_{av}[b]	2.122(5)	Cr(2)–N_{av}[b]	2.014(5)
Cr(3)–N_{av}[b]	2.120(5)	Cr(4)–N_{av}[b]	2.025(5)
Cr(1)–Cr(2)–Cr(1A)	178.72(7)	Cr(3)–Cr(4)–Cr(3B)	178.21(7)
C1(1)–Cr(1)–Cr(2)	179.54(6)	Cl(2)–Cr(3)–Cr(4)	178.48(6)
N–Cr–Cr–N Torsion$_{av}$[b]	21.06		

[a] Symmetry operations A = $-x+1$, y, $-z+1/2$; B = $-x$, y, $-z+1/2$. [b] Average value from the four wrapping ligands. [c] Symmetry operations A = $-x$, y, $-z$; B = $-x-1$, y, $-z+1$.

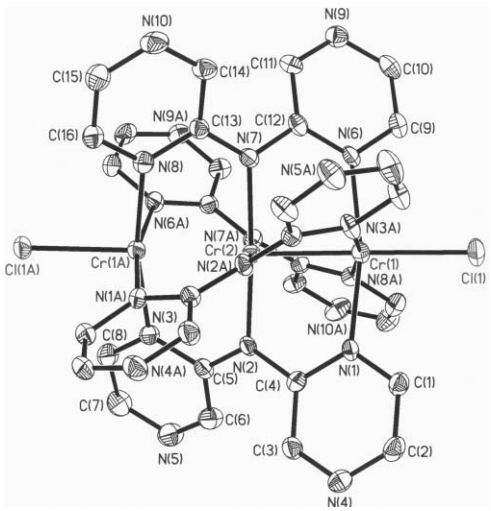

Fig. 6 Crystal structure of one $[Cr_3(\mu_3\text{-dpza})_4Cl_2]$ molecule in **6**·0.5CH_2Cl_2·0.5CH_3OH·H_2O. The hydrogen atoms have been omitted for clarity and thermal ellipsoids are at the 50% probability. Symmetry operations A = $-x$, y, $-z$.

complexes **4** and **6**, and in the asymmetric unit the central Ni or Cr atoms lie on twofold axes.

For nickel complexes **4** and **5**, the Ni–Ni distances are in the range 2.439–2.446 Å, with an average of 2.443 and 2.441 Å for **4** and **5**, respectively. The terminal nickel atoms are five coordinated with Ni–N_{av} distances of 2.091 and 2.077 Å for **4** and **5**, respectively, and consistent with high spin Ni(II). The central nickel atoms in both complexes are four-coordinated with four deprotonated amino nitrogen atoms in a square planar geometry with a Ni–N_{av} distance of 1.886 and 1.892 Å for **4** and **5**, respectively, and consistent with low spin Ni(II). There is no crystallographically imposed symmetry in **5**. A comparison of the bond lengths in the nickel and chromium trimetal EMAC is shown in Scheme 3.

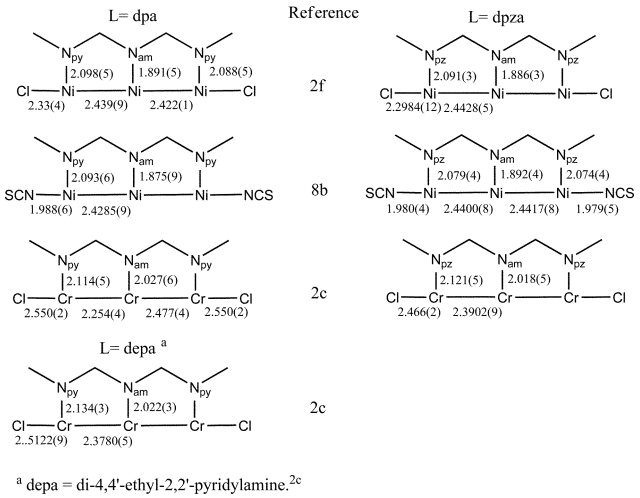

Scheme 3

The ^{1}H NMR spectrum of **4** in $CDCl_3$ solution showed three resonances at 53.8, 37.9 and 18.7 ppm (Fig. 7), with the intensities decreasing with increases of magnitude of contact shift. This result corresponds to the D_4 symmetry of structure with eight equivalent pyrazinyl groups in **4**.

Two kinds of structures, symmetrical and unsymmetrical configurations, have been found for chromium EMAC.[2c,13] The symmetrical structures exhibit all Cr–Cr bonds with equivalent distances of $d_{Cr-Cr} > 2.35$ Å, and the unsymmetrical structures consist of quadruple Cr–Cr bonds with $d_{Cr-Cr} < 2.3$ Å and a separated high spin Cr(II). For complex **6**, when we constrained the two Cr–Cr distances to be equal by the crystallographic 2-fold axis which passes through the center chromium atom, an excellently resolved symmetrical structure was obtained with a final R factor of 0.0591. Cr–Cr distances for two crystallographically independent molecules in a unit are 2.385(9) and 2.396(8) Å, respectively. The thermal ellipsoid for the central chromium atom was not elongated (Fig. 6). Thus, the structure of complex **6** can be described as a symmetrical structure, which indicates that the electron density is highly delocalized through the whole EMAC core.

This result is significantly different from that for the dipyridylamine complex $[Cr_3(\mu_3\text{-dpa})_4Cl_2]$ which showed $\Delta d_{Cr-Cr} > 0.22$ Å, but similar to the di-4,4′-ethyl-2,2′-pyridylamine (Hdepa) complex $[Cr_3(\mu_3\text{-depa})_4Cl_2]$ which is symmetrical. Berry and Cotton studied a series of trichromium(II) complexes and proposed that the structures can be tuned by the strength of the axial donor ligand and the basicity of equatorial ligands, with the more basic bridging ligand affecting the symmetry of the structure: Hdepa favors a symmetrical structure, whereas less basic ligand, Hdpa will lead to an unsymmetrical structure.[2c] Because there is only a slight

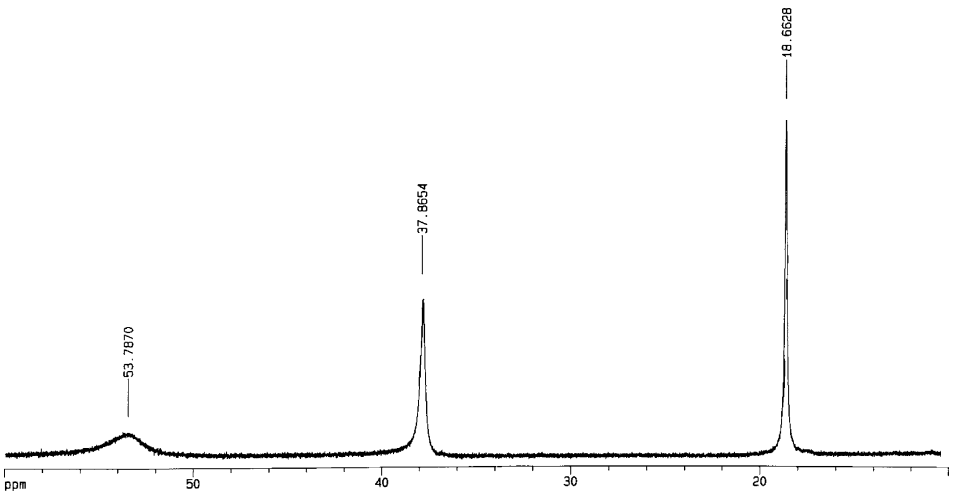

Fig. 7 ^{1}H NMR spectrum of **4** taken at 400 MHz in $CDCl_3$ solution.

difference of pK_b between pyridine and ethylpyridine (about 0.8), this conclusion remains in doubt, and requires more evidence. Complex **6**, with much less basic ligand Hdpza, produced a symmetrical structure in spite of the difference of pK_b between pyridine and pyrazine being more than 5. Thus, the electron factors of bridging ligand affecting the symmetrical and unsymmetrical structures are subtle and as yet unclear.

Last, it is worth noting that the Cr–Cl distance in trichromium(II) EMACs is apparently longer than that in Ni complexes, and the Cr–Cl distances in **6** are the shortest among trichromium chloride EMAC (Scheme 3).

Electrochemistry

The cyclic voltammograms of complexes **4–6** in solutions of CH_2Cl_2 in the range −1.6 to +1.6 V (Table 4) revealed that these complexes were very different electrochemically from the unsubstituted ligand, Hdpa complexes $[M_3(\mu_3\text{-dpa})_4X_2]$ (Fig. 8). While the CV of $[Ni_3(\mu_3\text{-dpa})_4Cl_2]$ showed one reversible couple at $E_{1/2} = +0.105$ V, a reversible redox couple for **4** was observed at $E = -0.504$ V. In the case where the axial ligand was NCS^-, a reversible reduction wave was observed at $E_{1/2} = -0.360$ V for **5**. When the solvent was changed to CH_3CN, the reduction peak for **4** was observed at $E_{1/2} = -0.540$ V. Thus introduction of pyrazine instead of pyridine to the trinickel complex resulted in an anodic shift of the redox couple, and made the complex $Ni_3(\mu_3\text{-dpza})_4Cl_2$ more resistant to oxidation. The same trend was found for trichromium complex **6** which had one reversible reduction wave at $E_{1/2} = -1.124$ V and two reversible oxidations at $E = +0.764$ and +1.400 V. Compared with the di(2-pyridyl)amine complex $[Cr_3(\mu_3\text{-dpa})_4Cl_2]$, which showed a redox wave at +0.18 and +0.95 V, **6** was much more stable to oxidation and could undergo reduction.[2c] The introduction of the pyrazine rings to the trichromium complex facilitates reduction and retards oxidation. This can be attributed to the fact that the pyrazine ring, containing two nitrogen atoms, is more electronegative than the pyridine ring.

Table 4 Comparison of the CV data (potential, V) for trimetal complexes of Hdpa and Hdpza

	$[Ni_3(L)_4Cl_2]$	$[Ni_3(L)_4(NCS)_2]$	$[Cr_3(L)_4Cl_2]$
L = dpza	−0.504	−0.360	+1.400, +0.764, −1.124
L = dpa	+0.105	+0.469[a]	+0.95, +0.18

[a] Irreversible process.

Magnetic properties

The magnetic susceptibility of complex **3** was measured over a temperature range of 2–300 K, and revealed a $\chi_M T$ value (product of molar magnetic susceptibility χ_M and temperature) of 3.2 emu K mol^{-1} at 300 K, a reasonable value for a high spin Co(II) ion with an important orbital contribution arising from the $^4T_{1g}$ ground state. Upon cooling, the $\chi_M T$ decreased continuously to a value of 1.90 emu K mol^{-1}, and the χ_M increased to a maximum of 1.06 emu mol^{-1} at 2 K. The curve obtained is shown in Fig. 9. Magnetic behavior showed that Hdpza mediates weak antiferromagnetic coupling in **3** *via* the *anti–syn* coordination mode.

The magnetic behavior of **4** and **5** were similar, with both exhibiting maximum χ_M at room temperature, as seen in Fig. 10. As the temperature was lowered, both χ_M decreased becoming negligible below 50 K, and then increased again. Complexes **4** and **5** gave $\chi_M T$ values at room temperature (300 K) of 1.09 and 1.04 emu K mol^{-1}, respectively, and these decreased continuously upon cooling. This is typical of antiferromagnetic behavior. The increase of χ_M at low temperature seen for complexes **4** and **5** was due to the noncoupled paramagnetic species. Therefore the magnetic results were consistent with the structural conclusion: two antiferromagnetically coupled high spin Ni(II), which are five-coordinated with square pyramidal geometry in terminal positions, and one diamagnetic low spin Ni(II), which is four-coordinated with square planar geometry in the central position. The maximum χ_M at room temperature suggests a strong magnetic interaction between the two terminal nickel atoms with $|J| \geq 200$ cm^{-1} according to $kT_{max}/|J| = 0.976$ for $S = 1$ system.

The temperature dependence of the molar magnetic susceptibility of **4** and **5** were fitted with a theoretical expression for a dinuclear system deduced from the spin Hamiltonian equation $\boldsymbol{H} = -J\boldsymbol{S}_1\boldsymbol{S}_2$ ($S_1 = S_2 = 1$), and modified to include a number of uncoupled species ($S = 1$), ρ. The experimental results were

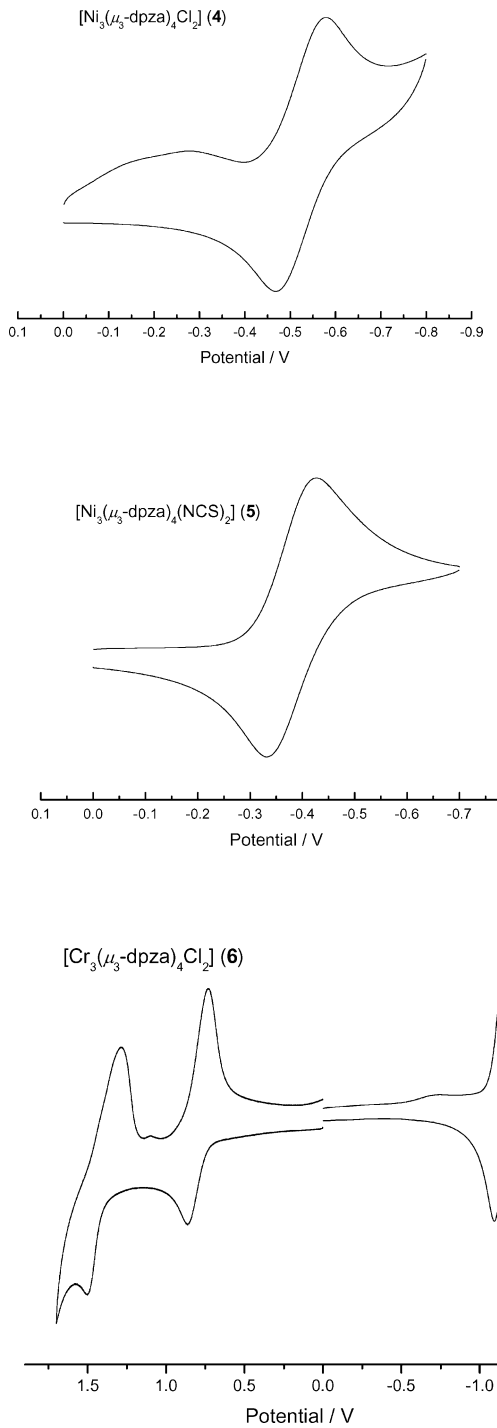

Fig. 8 The cyclic voltammograms of **4–6** in CH_2Cl_2 with 0.1 M TBAP.

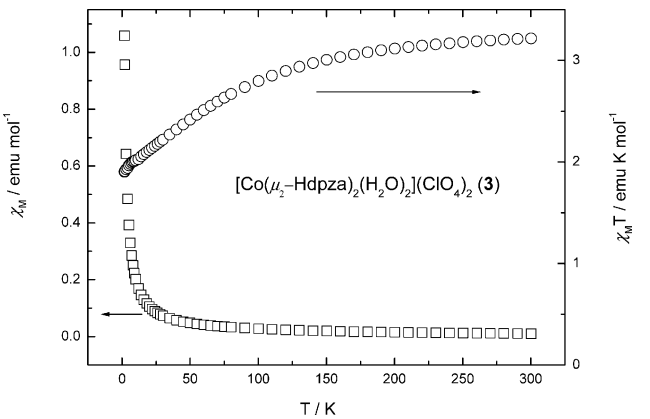

Fig. 9 Plots of $\chi_M T$ (○, right) and molar magnetic susceptibility χ_M (□, left) *vs.* T for compound **3**.

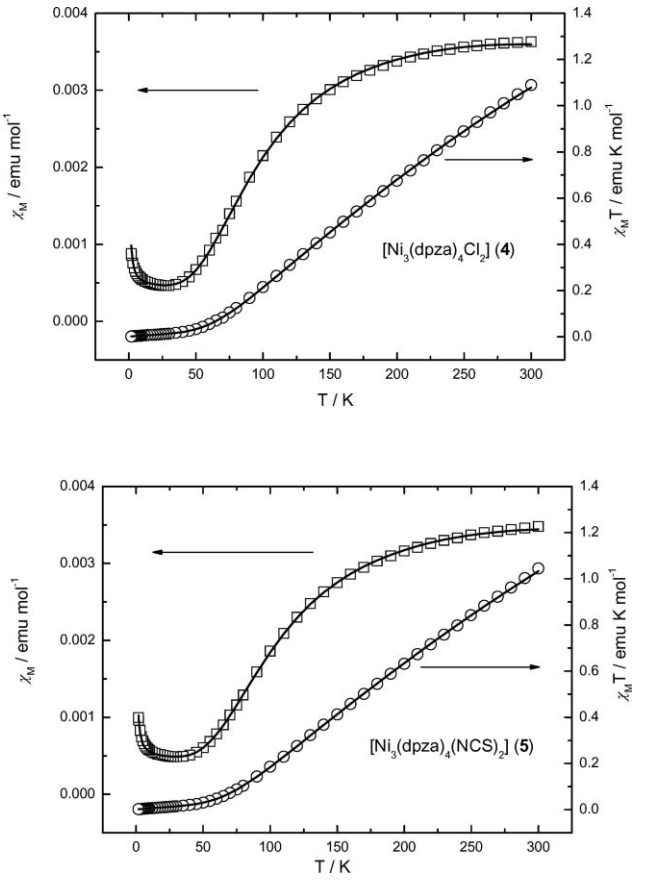

Fig. 10 Plots of molar magnetic susceptibility χ_M (□, left) and $\chi_M T$ (○, right) *vs.* T for compound **4** (top) and **5** (bottom). Solid lines result from least-squares fits using the eqn. (1) and (2).

in excellent agreement with the theoretical analyses (eqn. (1) and (2)). The J values were comparable with the references' values for $[Ni_3(\mu_3\text{-dpa})_4Cl_2]$ and $[Ni_3(\mu_3\text{-depa})_4Cl_2]$ (Table 5) in spite of the different electron configuration of the bridging ligands, which provides new evidence for superexchange occuring through the central nickel atoms.[2e,14]

$$\chi = \frac{2Ng^2\beta^2(e^{J/kT} + 5e^{3J/kT})}{kT(1 + 3e^{J/kT} + 5e^{3J/kT})} \quad (1)$$

$$\chi_\rho = \chi(1-\rho) + \frac{2Ng^2\beta^2\rho}{3kT}S(S+1) + \text{TIP} \quad (2)$$

The $\chi_M T$ value of complex **6** at room temperature (300 K) was 3.09 emu K mol^{-1}, which corresponded to a quintet ground state (Fig. 11). From 300 K to 15 K, $\chi_M T$ decreased very slightly, and was almost constant upon cooling. A fit of $1/\chi_M$ *versus* T with the Curie–Weiss equation for $S = 2$ gave $g = 2.05$ and

Table 5 Magnetic data for complexes **4** and **5**

	g	J/cm^{-1}	TIP ($\times 10^6$)	ρ (%)	F ($\times 10^{-7}$)[a]
$[Ni_3(\mu_3\text{-dpza})_4Cl_2]$(**4**)	2.154 ± 0.003	−200.5 ± 0.5	430 ± 5	0.041 ± 0.003	3.08
$[Ni_3(\mu_3\text{-dpza})_4(NCS)_2]$(**5**)	2.188 ± 0.003	−218.4 ± 0.5	470 ± 4	0.043 ± 0.002	1.47
$[Ni_3(\mu_3\text{-dpa})_4Cl_2]$[b]	2.067	−218.2	<300	<1	
$[Ni_3(\mu_3\text{-depa})_4Cl_2]$[b]	2.245	−217.5	<300	<1	

[a] F is defined as $\Sigma(\chi_{i\,exp})^{-1}(\chi_{i\,exp} - \chi_{i\,theo})^2$. [b] Data taken from ref. 15.

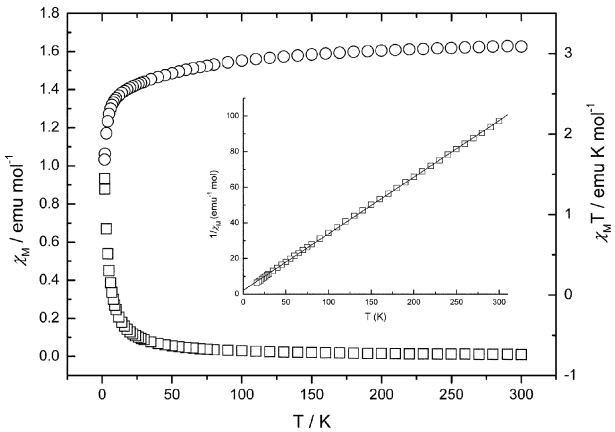

Fig. 11 Plots of molar magnetic susceptibility χ_M (□, left) and $\chi_M T$ (○, right) *vs.* T for compound **6**. Inset: Reciprocal dependence of the magnetic susceptibility on temperature. The solid lines result from least-square fits of the Curie–Weiss Law.

$\theta = -6.4$ K. An obvious decrease of $\chi_M T$ was observed below 15 K, which was due to zero-field splitting and intermolecular interactions. The θ value indicated a large magnitude of zero-field splitting, which was attributed to a strong interaction of electrons with delocalized molecular orbitals. Compared with the significant intramolecular antiferromagnetic coupling seen in the trinickel and tricopper EMACs with the same structure, this complex had an almost constant magnetic moment.[2d] This can be attributed to a quintet ground state with four delocalized unpaired electrons and a substantially high excited state.[2c] The structural analyses support this conclusion.

DFT calculations for complex **6** were performed. As in the electronic configuration of $[Cr_3(\mu_3\text{-dpa})_4Cl_2]$, which was carried out by Bénard, Rohmer and co-workers,[16] **6** can be described as a doubly occupied σ-bonding orbital, a singly occupied σ-nonbonding orbital and a set of singly occupied orbitals consisting of six π and three δ orbitals between the σ-bonding and σ-nonbonding orbitals. Since the π and δ orbitals are sensitive to the Cr–Cr distances, the sequence of the electronic configuration may vary as the Cr–Cr distance is changed. Thus, the ground state of the $[Cr_3(\mu_3\text{-dpza})_4Cl_2]$ may also change with different Cr–Cr distances. In order to decrease the influence of varying of the Cr–Cr distance, all calculations for complex **6** were performed using molecular coordination obtained by X-ray single-crystal structure. The calculated atomic spin population of the quintet state of **6** are listed in Chart 1, which is also similar to that of $[Cr_3(\mu_3\text{-dpa})_4Cl_2]$. Hence, the spin-coupling mechanism of **6** in the quintet state could be concluded qualitatively as $[Cr_3(\mu_3\text{-dpa})_4Cl_2]$.[16]

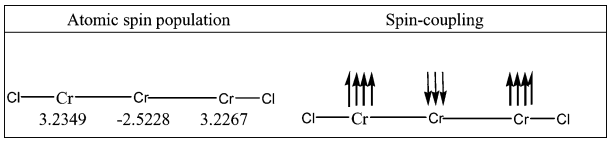

Chart 1 Atomic spin population and spin-coupling scheme for complex **6**.

Conclusions

The introduction of pyrazine to Hdpa instead of pyridine rings gives rise to a new versatile ligand not only for EMACs, but also for coordination polymers. Three types of coordination modes were found for the Hdpza complexes: *anti–anti* style resulted in a mononuclear compound **2**, *anti–syn* resulted in a 2-D coordination polymer **3**, and *syn–syn* was observed in the extended metal atom chains **4**, **5** and **6**. The structure of trichromium EMAC showed that the two Cr–Cr bond distances are very similar to each other. Electrochemical analysis revealed that complexes **4–6** have very different redox properties from those of Hdpa EMACs with all three of them being able to undergo reduction and being much more stable to oxidation, compared with complexes of Hdpa. Magnetic studies revealed that Hdpza mediates weak antiferromagnetic coupling when coordinated as the *anti–syn* bridging ligand in **3**, whereas the magnetic interaction parameter was greater than −200 cm^{-1} in the *syn–syn* coordinated, extended metal atom chains **4** and **5**. The magnetic results support a superexchange pathway in EMAC.

Experimental

Materials

All reagents and solvents were obtained from commercial sources and were used without further purification unless otherwise noted. The CH_2Cl_2 was dried over CaH_2 and freshly distilled prior to use.

Tetra-*n*-butylammonium perchlorate (TBAP) was recrystallized twice from ethyl acetate and dried under vacuum.

Physical measurements

Absorption spectra were recorded on a HEWLETT PACKARD 8453 spectrophotometer. IR spectra were performed with a Perkin Elmer FT–IR Spectrometer PARAGON 1000 in the range of 400–4000 cm^{-1}. ^{1}H NMR was recorded in $(CD_3)_2SO$ and chemical shifts were reported in ppm relative to $(CD_3)_2SO$ (δ 2.49 ppm for ^{1}H). FAB-MS mass spectra were obtained with a JEOL JMS-700 HF double focusing spectrometer operating in the positive

ion detection mode. Molar magnetic susceptibility was recorded in the range of 2–300 K on a SQUID system with 2000 G external magnetic field. Electrochemistry was performed with a three-electrode potentiostat (CH Instruments, Model 750A) in a CH_2Cl_2 solution deoxygenated by purging with prepurified nitrogen gas. Cyclic voltammetry was conducted with a three-electrode cell equipped with a BAS glassy carbon (0.07 cm^2) or platinum (0.02 cm^2) disk as the working electrode, a platinum wire as the auxiliary electrode, and a home-made Ag/AgCl (saturated) reference electrode. The reference electrode is separated from the bulk solution by a double junction filled with electrolyte solution. Potentials are reported *vs.* Ag/AgCl (saturated) and referenced to the ferrocene/ferrocenium (Fc/Fc^+) couple which occurs at $E_{1/2} = +0.54$ V *vs.* Ag/AgCl (saturated). The working electrode was polished with 0.03 μm aluminium on Buehler felt pads and was put under ultrasonic radiation for 1 min prior to each experiment. The reproducibility of individual potential values was within ± 5 mV.

Preparation of compounds

Di(pyrazin-2-yl)amine (Hdpza) (1). The reaction of aminopyrazine (9.51 g, 0.10 mol) and chloropyrazine (11.45 g, 0.10 mol) in the presence of $Pd_2(dba)_3$ (1.83 g, 2 mol%), BINAP (2.49 g, 4 mol%) and Bu^tONa (13.45 g, 1.40 mol) in benzene (250 mL) for 72 h gave a crude product of **1**. Purification by column chromatography over silica gel (dichloromethane–acetone, 10 : 1) gave colorless crystals of **1** after evaporation (12.1 g, 70% yield). mp 215–216 °C; IR (KBr) $\nu/cm^{-1} = 3234$ w, 3188 w, 3140 w, 3092 w, 3018 w, 2964 w, 2932 w, 2858 w, 1618 m, 1586 m, 1530 s, 1429 s, 1316 m, 1152 m, 1072 m, 1004 m, 832 s, 418 m, 412 m; UV/Vis (CH_3OH) λ_{max}/nm ($\varepsilon/dm^3\ mol^{-1}\ cm^{-1}$) = 221 ($9.21 \times 10^3$), 267 ($3.04 \times 10^4$), 338 ($2.20 \times 10^4$); ^1H NMR (400 MHz, $(CD_3)_2SO$): δ 10.33 (s, 1 H), 8.26, (s, 2H), 8.98-8.97 (d, $J = 0.84$ Hz, 2H), 8.14-8.13 (d, $J = 2.52$ Hz, 2H); EA (%) $C_8H_7N_5$: calcd. C 55.5, H 4.1, N 40.4; found: C 55.3, H 3.9, N 40.4.

$[Cu(Hdpza)_2(H_2O)_2](ClO_4)_2$ (2). A mixture of Hdpza (0.10 g, 0.58 mmol) and $Cu(ClO_4)_2{\cdot}6H_2O$ (0.24 g, 0.65 mmol) in methanol (50 mL) was stirred overnight. Then the solution was filtered to remove insoluble impurities and concentrated under vacuum. Slow evaporation of the solution gave green crystals suitable for X-ray diffraction (0.11 g, 59% yield (on the basis of Hdpza)). IR (KBr) $\nu/cm^{-1} = 3557$ m, 3300 s, 3244 s, 3182 s, 3114 m, 1634 m, 1567 w, 1505 vs, 1471 m, 1411 m, 1398 m, 1356 w, 1308 w, 1186 m, 1174 m, 1155 s, 1109 s, 1082 s, 1042 m, 934 w, 924 w, 867 w, 841 m, 668 w, 625 m, 454 m; UV/Vis (DMSO) λ_{max}/nm ($\varepsilon/dm^3\ mol^{-1}\ cm^{-1}$) = 274 ($4.11 \times 10^4$), 339 ($3.45 \times 10^4$), 433 (71.6), 804 (29.5); EA (%) $C_{16}H_{18}N_{10}O_{10}Cl_2Cu{\cdot}2H_2O$: calcd. C 28.2, H 3.3, N 20.6; found: C 28.2, H 3.2, N 20.4.

$[Co(\mu_2\text{-}Hdpza)_2(NCS)_2]$ (3). A mixture of Hdpza (80 mg, 0.46 mmol), $Co(NCS)_2$ (80 mg, 0.46 mmol) and methanol (60 mL) was stirred for 1 day. The resulting pink precipitate was filtered off. Slow evaporation of the filtrate gave hexagonal crystals suitable for X-ray diffraction (90 mg, 75% yield). IR (KBr) ν/cm^{-1} = 3231 m, 3129 w, 3055 w, 2967 w, 2922 w, 2878 w, 2077 vs, 1605 m, 1593 m, 1553 m, 1512 s, 1481 m, 1420 s, 1314 s, 1261 w, 1192 m, 1171 m, 1154 m, 1080 w, 1023 w, 1016 m, 912 w, 840 w, 830 m, 804 w, 740 w, 632 w, 550 w, 431 m; UV/Vis (DMSO) λ_{max}/nm ($\varepsilon/dm^3\ mol^{-1}\ cm^{-1}$) = 274 ($3.74 \times 10^4$), 299 ($1.37 \times 10^4$), 341 ($3.06 \times 10^4$), 421 (46.6), 486 (20.8), 538 (28.9), 623 (1.23×10^3); EA (%) $C_{18}H_{14}N_{12}\ CoS_2H_2O$: calcd. C 40.1, H 3.0, N 31.2; found: C 40.4, H 2.8, N 30.7.

$[Ni_3(\mu_3\text{-}dpza)_4Cl_2]$ (4). Anhydrous $NiCl_2$ (0.62 g, 4.8 mmol), Hdpza (1.00 g, 5.78 mmol) and naphthalene (30 g) were placed in an Erlenmeyer flask. The mixture was heated (about 170–180 °C) for 12 h under argon. Then a solution of potassium *tert*-butoxide (0.71 g, 6.35 mmol) in *n*-butyl alcohol (4 mL) was added dropwise. The mixture was refluxed for 6 h continuously. After the mixture had cooled, hexane was added to wash out naphthalene. The solid powder was extracted with CH_2Cl_2 and recrystallized from $CHCl_3$–ethyl ether solution, and deep blue–purple crystals were obtained (0.27 g, 20% yield). IR (KBr) ν/cm^{-1} = 3442 m, br, 3085 w, 3048 w, 3010 w, 1512 w, 1494 m, 1474 s, 1462 s, 1410 s, 1354 m, 1324 w, 1289 w, 1194 w, 1144 s, 1064 w, 1026 m, 832 w, 447 m; UV/Vis (CH_3OH) λ_{max}/nm ($\varepsilon/dm^3\ mol^{-1}\ cm^{-1}$) = 251 ($4.40 \times 10^4$), 297 ($4.57 \times 10^4$), 362 ($4.49 \times 10^4$), 534 ($3.43 \times 10^3$); MS (FAB): *m/z* (%) 926 (12) $[M]^+$, 891 (25) $[M–Cl]^+$; EA (%) $[Ni_3(dpza)_4Cl_2]{\cdot}H_2O$: calcd. C 40.3, H 2.8, N 29.4; found: C 40.7, H 2.6, N 28.9.

$[Ni_3(\mu_3\text{-}dpza)_4(NCS)_2]$ (5). $[Ni_3(\mu_3\text{-}dpza)_4Cl_2]$ (0.50 g, 0.53 mmol) and NaNCS (0.43 g, 5.30 mmol) were placed in an Erlenmeyer flask in CH_2Cl_2 (100 mL). The blue–purple solution was stirred for 3 d. Then water (20 mL) was added to dissolve unreacted NaNCS. The solution was extracted with CH_2Cl_2 (4 × 80 mL). Na_2SO_4 was added to the organic layer to remove the water. The CH_2Cl_2 solution was concentrated, and blue–purple powder was obtained. The powder was recrystallized from $CHCl_3$–ethyl ether solution, and deep blue–purple crystals were obtained (0.45 g, 86% yield). IR (KBr) ν/cm^{-1} = 3438 m, br, 3086 w, 3048 w, 3010 w, 2075 vs, 1513 w, 1496 m, 1472 s, 1417 s, 1358 m, 1320 w, 1288 w, 1190 w, 1145 s, 1066 w, 1028 m, 818 w, 446 m; UV/Vis (CH_3OH) λ_{max}/nm ($\varepsilon/dm^3\ mol^{-1}cm^{-1}$) = 249 ($4.22 \times 10^4$), 297 ($4.44 \times 10^4$), 359 ($4.13 \times 10^4$), 538 ($3.16 \times 10^3$); MS (FAB): *m/z* (%) 981 (1) $[M]^+$, 922 (2) $[M–NCS]^+$; EA (%) $[Ni_3(dpza)_4(NCS)_2]{\cdot}0.5CH_2Cl_2$: calcd. C 40.5, H 2.5, N 30.1; found: C 40.7, H 2.3, N 29.6.

$[Cr_3(\mu_3\text{-}dpza)_4Cl_2]$ (6). Anhydrous $CrCl_2$ (0.40 g, 3.25 mmol), Hdpza (0.50 g, 2.89 mmol) and naphthalene (40 g) were placed in an Erlenmeyer flask. The mixture was heated (about 160–170 °C) for 10 h under argon and then a solution of potassium *tert*-butoxide (0.36 g, 3.20 mmol) in *n*-butyl alcohol (4 mL) was added dropwise. After the mixture had cooled, *n*-hexane was added to wash out the naphthalene. The remaining solid was extracted with CH_2Cl_2 and recrystallized from $CHCl_3$/ethyl ether. A deep brown crystal was then obtained (0.20 g, 30% yield). IR (KBr) ν/cm^{-1} = 3420m, br, 3091 w, 2078 w, 1524 w, 1472 s, 1427 s, 1357 w, 1323 w, 1196 w, 1151 m, 1063 w, 1027 m, 828 w, 756 w, 450 m; UV/Vis (CH_3OH) λ_{max}/nm ($\varepsilon/dm^3\ mol^{-1}cm^{-1}$) = 264 ($4.42 \times 10^4$), 290 ($2.86 \times 10^4$), 333 ($2.69 \times 10^4$), 397 ($2.04 \times 10^4$), 468 ($5.51 \times 10^3$), 557 ($1.88 \times 10^3$), 627 ($1.51 \times 10^3$), 730 ($2.35 \times 10^3$); EA (%) $[Cr_3(dpza)_4Cl_2]{\cdot}CH_2Cl_2$: calcd. C 39.6, H 2.6, N 28.0; found: C 40.1, H 2.9, N 27.8.

Table 6 Crystal data for **1–6**

Compound	Hdpza (**1**)	$[Cu(Hdpza)_2(H_2O)_2]\cdot(ClO_4)_2\cdot 2H_2O$ (**2**·$2H_2O$)	$[Co(\mu_2\text{-}Hdpza)_2(NCS)_2]$ (**3**)	$[Ni_3(\mu_3\text{-}dpza)_4Cl_2]\cdot 0.75C_4H_{10}O\cdot 0.25CH_2Cl_2$ (**4**·$0.75C_4H_{10}O\cdot 0.25CH_2Cl_2$)	$[Ni_3(\mu_3\text{-}dpza)_4(NCS)_2]\cdot 0.5H_2O$ (**5**·$0.5H_2O$)	$[Cr_3(\mu_3\text{-}dpza)_4Cl_2]\cdot 0.5CH_3OH\cdot H_2O\cdot 0.5CH_2Cl_2$ (**6**·$0.5CH_2Cl_2\cdot 0.5CH_3OH\cdot H_2O$)
Formula	$C_8H_7N_5$	$C_{16}H_{32}Cl_2CuN_{10}O_{12}$	$C_{18}H_{14}CoN_{12}S_2$	$C_{35.25}H_{32}Cl_{2.50}N_{20}Ni_3O_{0.75}$	$C_{34}H_{25}N_{22}Ni_3O_{0.5}S_2$	$C_{33}H_{29}Cl_5Cr_3N_{20}O_{1.5}$
Formula weight	173.19	680.88	521.46	1012.56	990.01	992.11
Temp/K	295(2)	295(2)	150(1)	150(1)	150(2)	150(1)
Crystal system	Orthorhombic	Orthorhombic	Monoclinic	Monoclinic	Orthorhombic	Monoclinic
Space group	$Pca2_1$	$Pbca$	$P2_1/n$	$P2/c$	$Pbca$	$P2$
a/Å	11.9865(7)	15.1795(4)	9.2206(2)	19.2247(3)	18.4859(3)	13.7908(3)
b/Å	3.7315(2)	10.8102(3)	7.7428(2)	10.3082(2)	16.6988(3)	10.3096(2)
c/Å	17.5501(11)	15.3382(4)	14.8613(3)	21.5836(4)	25.1757(4)	14.7425(3)
β/°	90	90	93.7248(12)	108.0440(13)	90	96.5009(11)
Volume/Å^3, Z	784.97(8), 4	2516.90(12), 4	1058.76(4), 2	4066.90(13), 4	7771.5(2), 8	2082.58(7), 2
D_c/Mg m^{-3}	1.465	1.797	1.636	1.654	1.692	1.582
Absorption coefficient/mm^{-1}	0.099	1.163	1.044	1.598	1.609	1.019
Crystal size/mm	0.80 × 0.08 × 0.02	0.18 × 0.16 × 0.10	0.10 × 0.05 × 0.05	0.25 × 0.13 × 0.05	0.20 × 0.14 × 0.08	0.33 × 0.08 × 0.02
θ range for data collection/°	2.32 to 27.49	2.66 to 25.00	2.53 to 27.50	1.11 to 27.50	1.62 to 27.50	1.39 to 27.50
Reflection collected	6426	2216	13071	42288	61025	21559
Independent reflections	1798	2216	2422	9312	8917	8791
	[R(int) = 0.0671]	[R(int) = 0]	[R(int) = 0.0615]	[R(int) = 0.0870]	[R(int) = 0.0870]	[R(int) = 0.0588]
R_1, $Rw_2[I > 2\sigma(I)]$	0.0546, 0.1212	0.0343, 0.0903	0.0762, 0.2430	0.0489, 0.1082	0.0586, 0.1470	0.0591, 0.1604
R_1, Rw_2 (all data)	0.0647, 0.1266	0.0448, 0.0973	0.0947, 0.2518	0.1128, 0.1335	0.1210, 0.1808	0.0908, 0.1788
GOF	1.082	1.058	1.254	0.0977	1.076	1.018

Crystal structure determinations

The chosen crystals were mounted on a glass fiber. Data collections were carried out on a BRUKER SMART Apex CCD at room temperature for **1** and **2** and on a NONIUS Kappa CCD diffractometer at 150 K for **3–6** using a Mo-Kα radiation (λ = 0.71073 Å) and a liquid nitrogen low-temperature controller. Cell parameters were retrieved and refined using the Bruker SMART for **1** and **2** and the DENZO-SMN software for **3–6** on all reflections. Data reduction was performed on the Bruker SAINT for **1** and **2** and on the DENZO-SMN software for **3–6**. Semi-empirical absorption corrections were applied for **1–6**. All the structures were solved by using the SHELXLS-97[17] and refined with SHELXLS-97[18] by full-matrix least squares on F^2 values. The detailed crystal data are listed in Table 6.

CCDC reference numbers 633377 (**1**), 633378 (**2**), 633379 (**3**), 633380 (**4**), 637998 (**5**) and 633381 (**6**).

For crystallographic data in CIF or other electronic format see DOI: 10.1039/b700533d

Acknowledgements

The authors would like to thank the National Science Council of the Republic of China for financial support and Mr Shih-Chi Wang for his help with magnetic measurement.

References

1 (*a*) E.-C. Yang, M.-C. Cheng, M.-S. Tsai and S.-M. Peng, *J. Chem. Soc., Chem. Commun.*, 1994, 2377; (*b*) S.-J. Shieh, C.-C. Lin, I. Chao, C.-C. Wang and S.-M. Peng, *Chem. Commun.*, 1996, 315; (*c*) C.-K. Kuo, J.-C. Chang, C.-Y. Yeh, G.-H. Lee, C.-C. Wang and S.-M. Peng, *Dalton Trans.*, 2005, 3696; (*d*) T.-B. Tsao, G.-H. Lee, C.-Y. Yeh and S.-M. Peng, *Dalton Trans.*, 2003, 1465.

2 (*a*) R. Clérac, F. A. Cotton, L. M. Daniels, K. R. Dunbar, K. Kirschbaum, C. A. Murillo, A. A. Pinkerton, A. J. Schutz and X. Wang, *J. Am. Chem. Soc.*, 2000, **122**, 6226; (*b*) R. Clérac, F. A. Cotton, K. R. Dunbar, T. Lu, C. A. Murillo and X. Wang, *J. Am. Chem. Soc.*, 2000, **122**, 2272; (*c*) J. F. Berry, F. A. Cotton, T. Lu, C. A. Murillo, B. K. Roberts and X. Wang, *J. Am. Chem. Soc.*, 2004, **126**, 7082; (*d*) J. F. Berry, F. A. Cotton, L. M. Daniels, C. A. Murillo and X. Wang, *Inorg. Chem.*, 2003, **42**, 2418; (*e*) J. F. Berry, F. A. Cotton and C. A. Murillo, *Dalton Trans.*, 2003, 3015; (*f*) R. Clérac, F. A. Cotton, K. R. Dunbar, C. A. Murillo, I. Pascual and X. Wang, *Inorg. Chem.*, 1999, **38**, 2655.

3 (*a*) S.-Y. Lai, T.-W. Lin, Y.-H. Chen, C.-C. Wang, G.-H. Lee, M.-H. Yang, M.-K. Leung and S.-M. Peng, *J. Am. Chem. Soc.*, 1999, **121**, 250; (*b*) F. A. Cotton, L. M. Daniels, C. A. Murillo and X. Wang, *Chem. Commun.*, 1998, 39.

4 (*a*) S.-J. Shieh, C.-C. Chou, G.-H. Lee, C.-C. Wang and S.-M. Peng, *Angew. Chem., Int. Ed. Engl.*, 1997, **36**, 56; (*b*) C.-C. Wang, W.-C. Lo, C.-C. Chou, G.-H. Lee, J.-M. Chen and S.-M. Peng, *Inorg. Chem.*, 1998, **37**, 4059; (*c*) C. Y. Yeh, C. H. Chou, K. C. Pan, C. C. Wang, G. H. Lee, Y. O. Su and S. M. Peng, *J. Chem. Soc., Dalton Trans.*, 2002, 2670; (*d*) J. F. Berry, F. A. Cotton, P. Lei, T. Lu and C. A. Murillo, *Inorg. Chem.*, 2003, **42**, 3534; (*e*) H.-C. Chang, J.-T. Li, C.-C. Wang, T.-W. Lin, H.-C. Lee, G.-H. Lee and S.-M. Peng, *Eur. J. Inorg. Chem.*, 1999, 1243.

5 (*a*) C.-H. Chien, J.-C. Chang, C.-Y. Yeh, G.-H. Lee, J.-M. Fang, Y. Song and S.-M. Peng, *Dalton Trans.*, 2006, 3249; (*b*) C.-H. Chien, J.-C. Chang, C.-Y. Yeh, G.-H. Lee, J.-M. Fang and S.-M. Peng, *Dalton Trans.*, 2006, 2106.

6 (*a*) Y.-H. Chen, C.-C. Lee, C.-C. Wang, G.-H. Lee, S.-Y. Lai and S.-M. Peng, *Chem. Commun.*, 1999, 1667; (*b*) S.-Y. Lai, C.-C. Wang, Y.-H. Chen, C.-C. Lee, Y.-H. Liu and S.-M. Peng, *J. Chin. Chem. Soc.*, 1999, **46**, 477; (*c*) W.-Z. Wang, R. H. Ismayilov, G.-H. Lee, I. P.-C. Liu, C.-Y. Yeh and S.-M. Peng, *Dalton Trans.*, 2007, 830.

7 (*a*) S.-M. Peng, C.-C. Wang, Y.-L. Jang, Y.-H. Chen, F.-Y. Li, C.-Y. Mou and M.-K. Leung, *J. Magn. Magn. Mater.*, 2000, **209**, 83; (*b*) R. H.

Ismayilov, W.-Z. Wang, R.-R. Wang, C.-Y. Yeh, G.-H. Lee and S.-M. Peng, *Chem. Commun.*, 2007, 1121.
8 (*a*) J. F. Berry, F. A. Cotton, L. M. Daniels and C. A. Murillo, *J. Am. Chem. Soc.*, 2002, **124**, 3212; (*b*) S.-Y. Lin, I.-W. P. Chen, C.-H. Chen, M.-H. Hsieh, C.-Y. Yeh, T.-W. Lin, Y.-H. Chen and S.-M. Peng, *J. Phys. Chem. B*, 2004, **108**, 959.
9 S. Aduldecha and B. Hathway, *J. Chem. Soc., Dalton Trans.*, 1991, 993.
10 R. H. Ismayilov, W.-Z. Wang, G.-H. Lee and S.-M. Peng, *Dalton Trans.*, 2006, 478.
11 F. A. Cotton, L. M. Daniels, J. T. Jordan, IV and C. A. Murillo, *Polyhedron*, 1998, **17**, 589.
12 S. Wagaw and S. L. Buchwald, *J. Org. Chem.*, 1996, **61**, 7240.
13 (*a*) R. Clérac, F. A. Cotton, L. M. Daniels, K. R. Dunbar, C. A. Murillo and I. Pascual, *Inorg. Chem.*, 2000, **39**, 748; (*b*) R. Clérac, F. A. Cotton, L. M. Daniels, K. R. Dunbar, C. A. Murillo and I. Pascual, *Inorg. Chem.*, 2000, **39**, 752; (*c*) R. Clérac, F. A. Cotton, L. M. Daniels, K. R. Dunbar, C. A. Murillo and I. Pascual, *Inorg. Chem.*, 2000, **39**, 3414.
14 P. Kiehl, M.-M. Rohmer and M. Bénard, M., *Inorg. Chem.*, 2004, **43**, 3151.
15 J. F. Berry, F. A. Cotton, T. Lu, C. A. Murillo and X. Wang, *Inorg. Chem.*, 2003, **42**, 3595.
16 (*a*) N. Benbellat, M.-M. Rohmer and M. Bénard, *Chem. Commun.*, 2001, 2368; (*b*) M.-M. Rohmer and M. Bénard, *J. Cluster Sci.*, 2002, **13**, 333.
17 G. M. Sheldrick, *SHELXS-97, Program for solution of crystal structures*, University of Göttingen, Germany, 1997.
18 G. M. Sheldrick, *SHELXL-97, Program for refinement of crystal structures*, University of Göttingen, Germany, 1997.